PHYSICAL REVIEW D **85,** 124016 (2012)

Apparent horizons in the quasispherical Szekeres models

Andrzej Krasiński

N. Copernicus Astronomical Centre, Polish Academy of Sciences, Bartycka 18, 00 716 Warszawa, Poland[*]

Krzysztof Bolejko

Astrophysics Department, University of Oxford, Oxford OX1 3RH, United Kingdom[†]

(Received 28 February 2012; published 11 June 2012)

The notion of an apparent horizon (AH) in a collapsing object can be carried over from the Lemaître-Tolman to the quasispherical Szekeres models in three ways: 1. Literally by the definition—the AH is the boundary of the region, in which every bundle of null geodesics has negative expansion scalar. 2. As the locus, at which null lines that are as nearly radial as possible are turned toward decreasing areal radius R. These lines are in general nongeodesic. The name ''absolute apparent horizon'' (AAH) is proposed for this locus. 3. As the boundary of a region, where null *geodesics* are turned toward decreasing R. The name ''light collapse region'' is proposed for this region (which is three-dimensional in every space of constant t); its boundary coincides with the AAH. The AH and AAH coincide in the Lemaître-Tolman models. In the quasispherical Szekeres models, the AH is different from (but not disjoint with) the AAH. Properties of the AAH and light collapse region are investigated, and the relations between the AAH and the AH are illustrated with diagrams using an explicit example of a Szekeres metric. It turns out that an observer who is already within the AH is, for some time, not yet within the AAH. Nevertheless, no light signal can be sent through the AH from the inside. The analogue of the AAH for massive particles is also considered.

DOI: 10.1103/PhysRevD.85.124016 PACS numbers: 04.20.Jb, 04.20.Gz, 04.70.Bw

I. MOTIVATION

This paper deals with the relationship between analogues of an apparent horizon (AH) that exist in the quasispherical Szekeres models [1–21] of the $\beta' \neq 0$ family.[1] The AH was first defined by Hawking and Ellis (HE, [24], in what follows we quote from this source) as the outer boundary of a connected component of an outer trapped region within a partial Cauchy surface $\mathcal{S}(\tau)$. A trapped region is the collection of all points $q \in \mathcal{S}(\tau)$ such that there exists an outer trapped surface $\mathcal{P} \subset \mathcal{S}(\tau)$ containing q. An outer trapped surface is a 2-surface in $\mathcal{S}(\tau)$ such that the family of outgoing null geodesics orthogonal to it has nonpositive expansion scalar, as defined by Sachs [18]. In our case, the partial Cauchy surfaces will be the hypersurfaces of constant t. It is a simple and rather small step forward from this definition to consider the collection of all apparent horizons in the sense of HE, and retain the name AH for the three-dimensional hypersurface thus formed. We shall use the term AH in the latter sense. Szekeres [2] showed that in his quasispherical model the AH in this broader sense is located at $R = 2M$ (in our notation). (He did not use the term ''AH.'') Hellaby and Krasiński [15] gave the name of AH to a different entity, for which the name ''absolute apparent horizon'' (AAH) is proposed here. The AAH is defined in terms of *nongeodesic* null lines that are, in a sense to be defined in Sec. IV, as nearly radial as possible. (Strictly radial curves do not exist in general Szekeres models because of their lack of symmetry [25].) The AAH is the locus at which these nearly radial null curves are turned toward decreasing areal radius R. In the Lemaître [26]-Tolman [27] (L-T) model, which is the spherically symmetric limit of the Szekeres models considered here, the AAH coincides with the AH [28], and the curves defining the AAH become radial null geodesics.

One more analogue of AH results when we consider null geodesics and the region, where they are turned toward decreasing R. For this region, the name ''light collapse region'' (LCR) is proposed here. Unlike AAH and AH, which are three-dimensional hypersurfaces in spacetime, the LCR is a four-dimensional subset of spacetime because the family of geodesics defining it is not uniquely determined.

The existence of the AAH is proven for every collapsing quasispherical Szekeres model in Sec. IV. In Sec. V, the LCR is defined and it is shown that the three-dimensional future boundary of LCR coincides with the AAH. In Sec. VI an explicit subcase of the quasispherical Szekeres model is chosen for a detailed investigation. We illustrate the relation between the AH and the AAH by diagrams showing their positions in space. It turns out that, for some directions, an observer who is already within the AH is, for some time, not yet within the AAH. The analogue of AAH for massive particles is also considered. In

[*]akr@camk.edu.pl

[†]Krzysztof.Bolejko@astro.ox.ac.uk

[1]In the literature there are several definitions of different kinds of horizons. Some of them require asymptotic flatness, others noninteraction with the surroundings. These do not apply here because of the dynamical character of the Szekeres spacetime. For different types of horizons and discussion the reader is referred to [22,23].

Sec. VII the matching of the quasispherical Szekeres solutions to the Schwarzschild solution is considered. It is shown that it is the AH that matches to the Schwarzschild event horizon located at $r = 2m$ and that the outgoing part of the AH is necessarily spacelike, so light rays cannot traverse it outwards from the inside. Both these facts indicate that the AH rather than the AAH is the true horizon.

The aim of this paper is to gain more insight into the geometry of the Szekeres solutions.

II. INTRODUCING THE $\beta' \neq 0$ QUASISPHERICAL SZEKERES SOLUTIONS

In this section, basic facts about the $\beta' \neq 0$ quasispherical Szekeres solutions are recalled for reference, and to define the notation. We will use the parametrization introduced by Hellaby [29]. The metric of these solutions is

$$\mathcal{E} \overset{\text{def}}{=} \frac{S}{2}\left[\left(\frac{x-P}{S}\right)^2 + \left(\frac{y-Q}{S}\right)^2 + 1\right],$$
$$ds^2 = dt^2 - \frac{(R_{,z} - R\mathcal{E}_{,z}/\mathcal{E})^2}{1+2E(z)}dz^2 - \frac{R^2}{\mathcal{E}^2}(dx^2 + dy^2), \quad (2.1)$$

where $E(z)$, $P(z)$, $Q(z)$, $S(z)$ are arbitrary functions, and $R(t, z)$ obeys the following equation; a consequence of Einstein's equations with dust source:

$$R_{,t}{}^2 = 2E(z) + \frac{2M(z)}{R} + \frac{1}{3}\Lambda R^2; \quad (2.2)$$

$M(z)$ being one more arbitrary function, and Λ being the cosmological constant. The coordinates of (2.1) are comoving, so the velocity field of the dust is $u^\mu = \delta^\mu_0$ and $\dot{u}^\mu = 0$. In the following we assume $\Lambda = 0$.

This solution has in general no symmetry, and reduces to the L-T solution when P, Q and S are all constant.[2] The sign of $E(z)$ determines the type of evolution; with $E(z_0) < 0$ the matter shell at $z = z_0$ expands away from an initial singularity and then recollapses to a final singularity, with $E(z_0) > 0$ the shell is ever-expanding or ever-collapsing, depending on the initial conditions; $E(z_0) = 0$ is the intermediate case, ever-expanding with asymptotically zero expansion velocity, or its time-reverse. All three evolution types may exist in different regions of the same spacetime. We consider here the recollapsing ($E < 0$) solution of (2.2) with $\Lambda = 0$,

$$R = -\frac{M}{2E}(1 - \cos\eta),$$
$$\eta - \sin\eta = \frac{(-2E)^{3/2}}{M}(t - t_B(z)), \quad (2.3)$$

where $t_B(z)$ is one more arbitrary function and $\eta(t, z)$ is a parameter. The mass-density in energy units is

$$\kappa\epsilon = \frac{2(M_{,z} - 3M\mathcal{E}_{,z}/\mathcal{E})}{R^2(R_{,z} - R\mathcal{E}_{,z}/\mathcal{E})}, \qquad \kappa \overset{\text{def}}{=} \frac{8\pi G}{c^4}. \quad (2.4)$$

For $\epsilon > 0$, $(M_{,z} - 3M\mathcal{E}_{,z}/\mathcal{E})$ and $(R_{,z} - R\mathcal{E}_{,z}/\mathcal{E})$ must have the same sign. Note that the sign may be flipped by the transformation $z \to -z$, so we may assume that $\mathcal{L} \overset{\text{def}}{=} R_{,z} - R\mathcal{E}_{,z}/\mathcal{E} > 0$ at least somewhere. Let us then consider whether $\mathcal{L}$ can change sign as a function of z. The set where $\mathcal{L} = 0$ is either (1) a curvature singularity (a shell crossing—see a comment on it in the next section) or (2), if it coincides with the set where $M_{,z} - 3M\mathcal{E}_{,z}/\mathcal{E} = 0$, an analogue of a neck, well-known from the L-T geometry [18]. Case (1) is excluded by assumption—we choose the functions in the model so that shell crossings do not occur. In case (2), the neck (if it exists) is a global feature of spacetime, and no ordinary astronomical object in our neighborhood is large enough to extend up to and through it. Thus, we assume that we are on one side of the neck, where

$$R_{,z} - R\mathcal{E}_{,z}/\mathcal{E} > 0 \Rightarrow M_{,z} - 3M\mathcal{E}_{,z}/\mathcal{E} > 0. \quad (2.5)$$

We also assume

$$M_{,z} > 0 \quad (2.6)$$

because the region where $M_{,z} < 0$ occurs is an analogue of the region behind the equator of a closed space in the positive-curvature Robertson-Walker spacetimes. Again, no astronomical object is that large.

The Robertson-Walker limit follows when $z = r$, $R(t, z) = rS(t)$, $E = E_0 r^2$, where $E_0 =$ constant and $P = Q = 0$, $S = 1$. This definition includes the definition of the limiting radial coordinate (the Szekeres model is covariant with the transformations $z = f(z')$, where $f(z')$ is an arbitrary function).

The quasispherical model may be imagined as such a generalization of the L-T model in which the spheres of constant mass were made nonconcentric. The functions $P(z)$, $Q(z)$ and $S(z)$ determine how the center of a sphere changes its position in a space $t =$ constant when the radius of the sphere is increased or decreased [15].

Within each single $\{t =$ constant, $z =$ constant$\}$ surface, which is a sphere, the (x, y) coordinates of (2.1) can be transformed to the spherical (ϑ, φ) coordinates by

$$(x - P, y - Q)/S = \cot(\vartheta/2)(\cos\varphi, \sin\varphi). \quad (2.7)$$

This transformation is called a *stereographic projection*. For its geometric interpretation see Refs. [15,18]. Using this transformation the factor $\mathcal{E}_{,z}/\mathcal{E}$ becomes

[2]The "$\beta' \neq 0$" refers to the fact that $e^\beta \overset{\text{def}}{=} R/\mathcal{E}$ depends on z, so $\beta' \equiv \beta_{,z} \neq 0$ (this notation follows Szekeres [1,2]). There exists another large family of Szekeres solutions, in which $\beta' = 0$. They require separate treatment and will not be considered here. See an extended presentation in Ref. [18], also for the associated quasiplane and quasihyperbolic Szekeres models.

$$\mathcal{E}_{,z}/\mathcal{E} = -[S_{,z}\cos\vartheta + \sin\vartheta(P_{,z}\cos\varphi + Q_{,z}\sin\varphi)]/S. \tag{2.8}$$

III. PROPERTIES OF THE QUASI-SPHERICAL SZEKERES SOLUTIONS

Definitions of the Szekeres solutions based on invariant properties can be found using Ref. [18].

Rotation and acceleration of the dust source are zero, the expansion is nonzero, the shear tensor is

$$\sigma^{\alpha}_{\beta} = \frac{1}{3}\Sigma\,\mathrm{diag}(0, 2, -1, -1), \qquad \text{where}$$
$$\Sigma = \frac{R_{,tz} - R_{,t}R_{,z}/R}{R_{,z} - R\mathcal{E}_{,z}/\mathcal{E}}. \tag{3.1}$$

The instant $t = t_B(z)$ in (2.3) is the Big Bang singularity corresponding to $R = 0$. When $t_{B,z} \neq 0$ (that is, in general) the instant of singularity is position-dependent.

Another singularity may occur where $R_{,z} - R\mathcal{E}_{,z}/\mathcal{E} = 0$ (if this equation has solutions for (x, y)). This is a shell crossing, but it is qualitatively different from that in the L-T model. As can be seen from (2.1), the equation $R_{,z} - R\mathcal{E}_{,z}/\mathcal{E} = 0$ can define at most a subset of an $\{x, y\}$ sphere. When a shell crossing exists, its intersection with a $t =$ constant space will be a circle, or, in exceptional cases, a single point (in L-T it is a whole sphere). For more on shell crossings in all the Szekeres solutions see Refs. [15,30]. They can be avoided if the functions and their derivatives obey a set of inequalities [15,21].

Equation (2.2) is formally identical with the Friedmann equation, but, with E and M depending on z, each surface $z =$ constant evolves independently of the others.

A quasispherical Szekeres region can be matched to the Schwarzschild solution across a $z =$ constant hypersurface [6].

The mass-density distribution given by (2.4) can be decomposed into the spherically symmetric monopole

$$\kappa\epsilon_S = \frac{2(M/\chi)^3}{(R/\chi)^2(R/\chi)_{,z}}, \tag{3.2}$$

where

$$\chi(z) \overset{\text{def}}{=} \frac{P^2 + Q^2 + S^2 + 1}{S}, \tag{3.3}$$

and the dipole

$$\kappa\Delta\epsilon = \frac{6MR_{,z} - 2M_{,z}R}{R^2(R_{,z}\chi - R\chi_{,z})} \times \frac{\chi_{,z} - \chi\mathcal{E}_{,z}/\mathcal{E}}{R_{,z} - R\mathcal{E}_{,z}/\mathcal{E}}. \tag{3.4}$$

The dipole is uniquely defined by the requirement that the surface where $\Delta\epsilon = 0$ (sure to exist, as follows from calculations—see Refs. [16,18]) passes through the center of symmetry of the monopole.[3]

[3]Equation (3.4) corrects a typo in Eqs. (2.194) and (2.196) of Ref. [16] and in Eq. (19.165) of Ref. [18]: one of the two appearances of Φ^2 in each equation should not be there.

IV. APPARENT VERSUS ABSOLUTE APPARENT HORIZONS IN THE QUASISPHERICAL SZEKERES MODELS

The results of this section were partly reported in Ref. [16]; the basic equations were introduced in Ref. [15].

An AH is the boundary of the region of trapped surfaces. A trapped surface S is one on which the families of outgoing null *geodesics* on both sides of S converge (i.e., have a negative expansion scalar). Thus, if k^{μ} is any field of vectors tangent to null geodesics that intersect S, then

$$k^{\mu}{}_{;\mu} < 0 \quad \text{on } S. \tag{4.1}$$

Consequently, on an AH:

$$k^{\mu}{}_{;\mu} = 0. \tag{4.2}$$

Proceeding from this definition, Szekeres [2] found that in a quasispherical model the AH is given by the same equation as in an L-T model:

$$R = 2M. \tag{4.3}$$

In an L-T model, (4.2) is equivalent to another definition: on an AH in collapsing matter, $R(z)$ calculated along an outgoing radial null geodesic changes from increasing to decreasing [18].

Hellaby and Krasiński [15] considered the analogue of an AH in a quasispherical Szekeres model, using this second definition, but for *nongeodesic* null fields defined below. We propose to name this the "absolute apparent horizon" (AAH)—because even a maximally accelerated ray cannot get out of it.

The reasoning was as follows. A general null direction $k^{\alpha} = \mathrm{d}x^{\alpha}/\mathrm{d}t$ in the metric (2.1) obeys[4]

$$\frac{(R_{,z} - R\mathcal{E}_{,z}/\mathcal{E})^2}{1 + 2E}\left(\frac{\mathrm{d}z}{\mathrm{d}t}\right)^2 = 1 - \frac{R^2}{\mathcal{E}^2}\left[\left(\frac{\mathrm{d}x}{\mathrm{d}t}\right)^2 + \left(\frac{\mathrm{d}y}{\mathrm{d}t}\right)^2\right]. \tag{4.4}$$

Thus, on a null curve with $\mathrm{d}x/\mathrm{d}t = 0 = \mathrm{d}y/\mathrm{d}t$ (which, in general, will not be a geodesic [16,17,25]), $|\mathrm{d}z/\mathrm{d}t|$ is maximal. Equation (4.4) implies, along this path:

$$\left.\frac{\mathrm{d}t}{\mathrm{d}z}\right|_n = \frac{j}{\sqrt{1 + 2E}}\left(R_{,z} - \frac{R\mathcal{E}_{,z}}{\mathcal{E}}\right), \qquad j = \pm 1, \tag{4.5}$$

where $j = +1$ for outgoing rays, and $j = -1$ for ingoing rays. Intuition suggests that along a curve (4.5) the light signal should escape farther from the "origin" $R = 0$ than along any other path. An example in Sec. VI will show that this is only partly true. Along some directions, the rays given by (4.5) can indeed proceed toward larger values of R even within the AH. But along the other directions the

[4]Along a null curve parametrized by an affine parameter s, the time coordinate t must obey $\mathrm{d}t/\mathrm{d}s > 0$ or $\mathrm{d}t/\mathrm{d}s < 0$ at all points (the curve would be spacelike at every point where $\mathrm{d}t/\mathrm{d}s = 0$). This shows that t can be used as a parameter on null geodesics (but in general it is not affine).

reverse happens: the rays (4.5) are redirected to decreasing values of R even outside the AH. The reason for this behavior is the fact that the two definitions of AH that are equivalent in the L-T limit are *inequivalent* in a Szekeres model: the locus where all bundles of light rays begin to converge is different from the locus where light rays are forced to collapse toward decreasing R, see Sec. V.

Let the solution of (4.5) be

$$t = t_n(z). \tag{4.6}$$

The value of R along this ray, $R_n(z) \overset{\text{def}}{=} R(t_n(z), z)$, is a monotonic function of z in some neighborhood of the emission point. The AAH is where $R_n(z)$ changes from increasing to decreasing or vice versa:

$$0 = \frac{\mathrm{d}R_n}{\mathrm{d}z} \equiv \frac{\partial R}{\partial t}\frac{\mathrm{d}t_n}{\mathrm{d}z} + \frac{\partial R}{\partial z} = \ell j \frac{\sqrt{2M/R + 2E}}{\sqrt{1+2E}}\left(R_{,z} - \frac{R\mathcal{E}_{,z}}{\mathcal{E}}\right) + R_{,z}, \tag{4.7}$$

from (2.2) and (4.5), where $\ell = +1$ for an expanding model and $\ell = -1$ for a collapsing model. We consider an AAH that is created in the collapse phase ($\ell = -1$), so it is defined by the outgoing rays ($j = +1$). Then, (4.7) becomes

$$R_{,z}\left(\frac{\sqrt{1+2E}}{\sqrt{2M/R+2E}} - 1\right) + R\frac{\mathcal{E}_{,z}}{\mathcal{E}} = 0. \tag{4.8}$$

In Ref. [15] it was found that in a constant-t space the AAH "is a kind of oval with half inside $R = 2M$ and half outside."[5] In Sec. VI we will investigate the relation of the AAH to the AH in a simple example of a recollapsing Szekeres model, and this will provide an illustration to the quoted statement.

We use the following expression for $R_{,z}$ (to be calculated from (2.3); see Eq. (18.107) in Ref. [18]):

$$\frac{R_{,z}}{R} = \left(\frac{M_{,z}}{M} - \frac{E_{,z}}{E}\right) + \left(\frac{3}{2}\frac{E_{,z}}{E} - \frac{M_{,z}}{M}\right)\frac{\sin\eta(\eta - \sin\eta)}{(1-\cos\eta)^2} - \frac{(-2E)^{3/2}}{M}t_{B,z}\frac{\sin\eta}{(1-\cos\eta)^2}. \tag{4.9}$$

We note from (2.2) and (2.3) that with $\pi \le \eta \le 2\pi$, where $R_{,t} < 0$, we have

$$\sqrt{2M/R + 2E} = -\sqrt{-2E}\frac{\sin\eta}{1-\cos\eta}. \tag{4.10}$$

We substitute (4.9) and (4.10) in (4.8), then multiply the result by $(1-\cos\eta)^2$ to avoid the infinite values at $\eta \to 0$ and $\eta \to 2\pi$, and obtain:

$$\Psi(\eta) \overset{\text{def}}{=} \left[\left(\frac{M_{,z}}{M} - \frac{E_{,z}}{E}\right)(1-\cos\eta)^{3/2} + \left(\frac{3}{2}\frac{E_{,z}}{E} - \frac{M_{,z}}{M}\right)\frac{\sin\eta(\eta-\sin\eta)}{\sqrt{1-\cos\eta}} - \frac{(-2E)^{3/2}}{M}t_{B,z}\frac{\sin\eta}{\sqrt{1-\cos\eta}}\right] \times \left[\sqrt{1+2E}\sqrt{1-\cos\eta} + \frac{\sqrt{-2E}\sin\eta}{\sqrt{1-\cos\eta}}\right] - \sqrt{-2E}\sin\eta(1-\cos\eta)\frac{\mathcal{E}_{,z}}{\mathcal{E}} = 0. \tag{4.11}$$

This determines $\eta(M, x, y)_{\text{AAH}}$. Then, from (2.3):

$$t(M, x, y)_{\text{AAH}} = \frac{M}{(-2E)^{3/2}}(\eta - \sin\eta)_{\text{AAH}} + t_B. \tag{4.12}$$

We assume that shell crossings are absent. Among the conditions for no shell crossings, found in Ref. [15], the following are useful here:

$$2\pi\left(\frac{3}{2}\frac{E_{,z}}{E} - \frac{M_{,z}}{M}\right) - \frac{(-2E)^{3/2}}{M}t_{B,z} < 0 \tag{4.13}$$

(see Eq. (126) in Ref. [15]), and

$$M_{,z}/M - E_{,z}/E > 0, \tag{4.14}$$

which follows from the fact that $R_{,z}/R > 0$ must hold for all (η, z), via (4.9) taken at $\eta = \pi$ [15]. We observe that

$$-\lim_{\eta\to 2\pi}\frac{\sin\eta}{\sqrt{1-\cos\eta}} = \sqrt{2} = \lim_{\eta\to 0}\frac{\sin\eta}{\sqrt{1-\cos\eta}}. \tag{4.15}$$

Now we verify using (4.11) that

$$\lim_{\eta\to\pi}\Psi(\eta) = 4\sqrt{1+2E}\left(\frac{M_{,z}}{M} - \frac{E_{,z}}{E}\right) > 0, \tag{4.16}$$

being positive in consequence of (4.14); and

$$\lim_{\eta\to 2\pi}\Psi(\eta) = 2\sqrt{-2E}\left[2\pi\left(\frac{3}{2}\frac{E_{,z}}{E} - \frac{M_{,z}}{M}\right) - \frac{(-2E)^{3/2}}{M}t_{B,z}\right] < 0, \tag{4.17}$$

being negative in consequence of (4.13).

Thus $\Psi(\pi) > 0$ and $\Psi(2\pi) < 0$, so there exists an $\eta_0 \in (\pi, 2\pi)$ at which $\Psi(\eta_0) = 0$, and it is unique (see Appendix A). In passing, we have proved that each particle in a recollapsing quasispherical Szekeres model must cross the AAH before it hits the Big Crunch at $\eta = 2\pi$.

[5] This can be easily seen from (4.8). Suppose, for definiteness, that $R_{,z} > 0$. Recall that $\mathcal{E} > 0$ (evident from (2.1)). Then $(\mathcal{E}_{,z} > 0) \Rightarrow (R < 2M)$, $(\mathcal{E}_{,z} = 0) \Rightarrow (R = 2M)$ and $(\mathcal{E}_{,z} < 0) \Rightarrow (R > 2M)$. For the proof that $\mathcal{E}_{,z}$ changes sign on an (x, y) sphere see Ref. [15]; $\mathcal{E}_{,z} = 0$ is a large circle on that sphere.

V. THE LIGHT COLLAPSE REGION (LCR) AND ITS FUTURE BOUNDARY

Consider a bundle of geodesic light rays flashed simultaneously from a common origin. Let v be the affine parameter along these rays, θ be the expansion scalar of the bundle, k^μ be the tangent vector field to the rays and δS be the surface area of the propagating front of the bundle. Then the following holds ([18], Eq. (16.131)):

$$k^\mu{}_{;\mu} \equiv 2\theta = \frac{\mathrm{d}}{\mathrm{d}v}\ln(\delta S). \tag{5.1}$$

Consequently, by (4.2), on an AH the δS stops increasing along the geodesics in the bundle defining the AH and begins to decrease. In an L-T model, a light front (LF) flashed from the origin $R = 0$ remains spherically symmetric at all times, and its surface area is proportional to R^2 calculated at the LF. Therefore, in a collapsing L-T model, the AH is at the same time the locus at which $R|_{\mathrm{LF}}$ reaches its maximum. *This coincidence between $\theta = 0$ and the maximum of $R|_{\mathrm{LF}}$ does not hold in a Szekeres model*, as is demonstrated below. The LF is not spherically symmetric, different points on it have different R values at a constant t, so the area of the front is no longer proportional to R^2. Thus, there may be locations where $\theta < 0$, but R is still increasing along the rays, and locations where $\theta > 0$ while R is decreasing. This remark should help in understanding the relation between AH and AAH discussed in Sec. VI.

This noncoincidence allows us to define one more entity related to AH, which we propose to name the "light collapse region" (LCR). This is the region where R has extrema along null geodesics, and so, during collapse, the rays are turned toward the Big Crunch.

Consider (4.4) along a null geodesic, and suppose we know the solution of the geodesic equations. Then (4.4) together with the geodesic equations defines the function

$$t = t_{ng}(z), \tag{5.2}$$

where "ng" stands for "along a null geodesic." For an outward-directed null geodesic we then have

$$\left.\frac{\mathrm{d}t}{\mathrm{d}z}\right|_{ng} = \left.\frac{R_{,z} - R\mathcal{E}_{,z}/\mathcal{E}}{\sqrt{1+2E}U}\right|_{ng}, \tag{5.3}$$

where

$$U \overset{\mathrm{def}}{=} \left.\sqrt{1 - \frac{R^2}{\mathcal{E}^2}\left[\left(\frac{\mathrm{d}x}{\mathrm{d}t}\right)^2 + \left(\frac{\mathrm{d}y}{\mathrm{d}t}\right)^2\right]}\right|_{ng}. \tag{5.4}$$

Proceeding exactly as from (4.6) to (4.8), and assuming we consider outward-directed null geodesics in the collapse phase of the model we arrive at the following analogue of (4.8)

$$\left.\frac{\mathrm{d}R}{\mathrm{d}z}\right|_{ng} = \frac{\sqrt{2M/R+2E}}{\sqrt{1+2E}U} \times \left.\left[R_{,z}\left(\frac{\sqrt{1+2E}U}{\sqrt{2M/R+2E}} - 1\right) + R\frac{\mathcal{E}_{,z}}{\mathcal{E}}\right]\right|_{ng}. \tag{5.5}$$

We define the LCR as the region where

$$\left.\frac{\mathrm{d}R}{\mathrm{d}z}\right|_{ng} = 0. \tag{5.6}$$

As stated before, the LCR is a four-dimensional subset of spacetime and a three-dimensional subset of a space of constant time. This is because the geodesics that define the LCR are not uniquely determined: the U in (5.4) depends on the direction of the geodesic considered and takes a range of values at a given (t, z).

Consider the intersection of LCR with the AAH, i.e. a locus where (4.8) and (5.6) hold simultaneously. Within this set we have $U = 1 \Rightarrow \mathrm{d}x/\mathrm{d}t = \mathrm{d}y/\mathrm{d}t = 0$. Thus, LCR $\bigcap$ AAH is a set in which both the nongeodesic null curves referred to in (4.5) and the null geodesics referred to in (5.3)–(5.4) begin to proceed toward decreasing R, and in addition the null geodesics happen to have $\mathrm{d}x/\mathrm{d}t = \mathrm{d}y/\mathrm{d}t = 0$ there, i.e. to be tangent to the curves defining the AAH. The definition of this set is identical to the definition of AAH, Eq. (4.8). This shows that the AAH is a boundary of the LCR. Actually, it is the future boundary, as we show below. Consider the collection of null geodesics that cross the AAH as defined by (4.8). For them, calculate (5.5) at the points that obey (4.8). It is convenient to rewrite (4.8) and (5.5) as follows:

$$R_{,z} - (R_{,z} - R\mathcal{E}_{,z}/\mathcal{E})\frac{\sqrt{2M/R+2E}}{\sqrt{1+2E}} = 0, \tag{5.7}$$

$$\left.\frac{\mathrm{d}R}{\mathrm{d}z}\right|_{ng} = R_{,z} - (R_{,z} - R\mathcal{E}_{,z}/\mathcal{E})\frac{\sqrt{2M/R+2E}}{\sqrt{1+2E}U}. \tag{5.8}$$

Using (5.7) in (5.8) we obtain

$$\beta \overset{\mathrm{def}}{=} \left.\frac{\mathrm{d}R}{\mathrm{d}z}\right|_{ng(\mathrm{AAH})} = (R_{,z} - R\mathcal{E}_{,z}/\mathcal{E})\frac{\sqrt{2M/R+2E}}{\sqrt{1+2E}}\left(1 - \frac{1}{U}\right). \tag{5.9}$$

Using (2.5), since $U \leq 1$ by construction, we see that $\beta \leq 0$. Those geodesics, for which $\beta = 0$ ($U = 1$) cross the AAH with $\mathrm{d}x/\mathrm{d}t = \mathrm{d}y/\mathrm{d}t = 0$ and are just being turned toward decreasing R. Those for which $\beta < 0$, while crossing the AAH are already proceeding toward decreasing R. This shows that the AAH lies at the future boundary of the LCR.

VI. EXPLICIT EXAMPLES OF AAH IN SZEKERES MODELS

A. Null rays

As an illustration, we take the recollapsing Szekeres model defined by the same equations that were used in Ref. [28] to discuss the formation of galactic-size black holes in the L-T model:[6]

$$t_B(M) = -bM^2 + t_{B0}, \tag{6.1}$$

$$t_C(M) = aM^3 + T_0 + t_{B0}, \tag{6.2}$$

where $t_B(M)$ is the bang time, $t_C(M)$ is the crunch time, a, b, t_{B0} and T_0 are arbitrary constants; t_{B0} is the time-coordinate of the central point of the Big Bang and T_0 is the time between the Big Bang and Big Crunch measured along the central line $M = 0$. Then, from (2.3), since $\eta = 2\pi$ at $t = t_C$:

$$2E(M) = -\frac{(2\pi M)^{2/3}}{(aM^3 + bM^2 + T_0)^{2/3}}. \tag{6.3}$$

As shown in Ref. [15], Eq. (185), the extreme values of $\mathcal{E}_{,z}/\mathcal{E}$ are

$$D_e \overset{\text{def}}{=} \frac{\mathcal{E}_{,z}}{\mathcal{E}}\bigg|_{\text{extreme}} = \pm\frac{\sqrt{S_{,z}^{\ 2} + P_{,z}^{\ 2} + Q_{,z}^{\ 2}}}{S}. \tag{6.4}$$

However, in choosing (P, Q, S) precaution must be taken not to make D_e too large. If it is too large, then either the numerator or the denominator of (2.4) becomes negative in a region of space, thus rendering the mass density negative there (and infinite where the denominator is zero). Physically, this means that the dipole component of (3.4) dominates over the monopole in that part of the space.

We thus first choose such a value of D_e that will make the difference between the graphs of AH and of AAH visible at the scale of a figure, and then we choose such P, Q and S that will imply the chosen value of D_e. To maximize D_e, at least one of the derivatives $P_{,z}$, $Q_{,z}$, $S_{,z}$ has to be large. Experiments showed that the following functions will yield the desired result:

$$a = 0.1, \qquad b = 5000, \qquad T_0 = 12.5, \qquad t_{B0} = 0,$$
$$S = M^{0.29}, \qquad P = 0.5M^{0.29}, \qquad Q = 0, \tag{6.5}$$

and $z' = M(z)$ was chosen as the new z-coordinate. The resulting AAH is shown in Fig. 1. The figure shows $t(M)$ on the AAH for two points in the (x, y) surface: the one where the D_e given in (6.4) is maximal (positive) and where it is minimal (negative). These two curves are compared with the ordinary AH and with the crunch time function $t_C(M)$. (This figure is a modification of Fig. 1 in Ref. [28].) See Appendix B for the proof that all four curves indeed have a common origin at $M = 0$.

Figure 1 shows that the contribution from $\mathcal{E}_{,z}/\mathcal{E}$ can either increase or decrease the region where the accelerated rays are forced toward the Big Crunch, depending on the direction. In the direction where this contribution is maximal (i.e. $\mathcal{E}_{,z}/\mathcal{E} > 0$—curve AAH−), the AAH appears later than the ordinary AH, and the term $\mathcal{E}_{,z}/\mathcal{E}$ causes that the accelerating ray can still proceed toward increasing R in a region where a geodesic bundle already converges. In the direction where D_e is minimal (i.e. $\mathcal{E}_{,z}/\mathcal{E} < 0$—curve AAH+), the AAH appears earlier than the AH, and the term $\mathcal{E}_{,z}/\mathcal{E}$ causes that the accelerating ray is turned inward where a geodesic bundle is still diverging.

Note what this means physically. A nongeodesic light ray is one that is guided by mirrors or optical fibers. When the AAH has a smaller radius than the AH, the observer who has already fallen into the AH still has a chance to send a message, using nongeodesic rays, to observers occupying loci with larger R. However, the nongeodesic ray has no chance to escape from inside the AH and will be turned toward the Big Crunch as well, only somewhat later than the geodesic one—see Sec. VII. Even this is possible only in some of the directions; in other directions the AAH is outside the AH and no ray within the AH, geodesic or not, can proceed toward larger R. (See later in this paper—Figs. 5 and 6 illustrate this point more clearly.)

Figure 2 shows a 3D graph of M on the AAH as a function of x and y, at the time instant $t = 13.0$ (compare to Fig. 1). All values of x and y are admissible, and at every

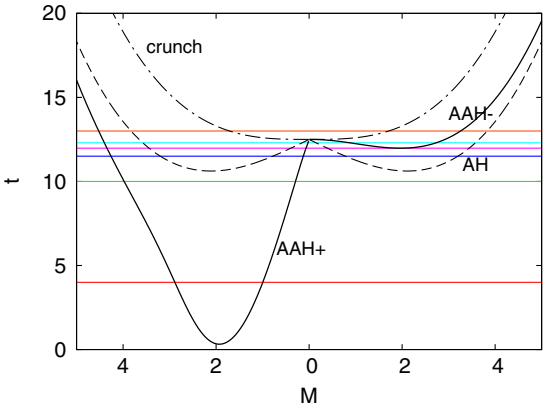

FIG. 1 (color online). A comparison of the future absolute apparent horizon (AAH) with the ordinary future apparent horizon (AH) in the model defined by (6.1) and (6.2). Curve AAH+ is the AAH along the direction where the contribution from $\mathcal{E}_{,z}/\mathcal{E}$ is maximal and curve AAH− is the AAH along the direction where this contribution is minimal. The dashed-dotted line represents the big crunch singularity. Horizontal solid lines show the instants for which the next figures are drawn, these are: $t = 4.0$, 10.0, 11.5, 11.9772, 12.3 and 13.0. Note that we use M as the radial coordinate.

[6]The values of the parameters a, b, T_0 and t_{B0} used here will be different from those in Ref. [28]. This model is meant to be an illustration to various geometrical possibilities; it is not supposed to describe any real object in the Universe.

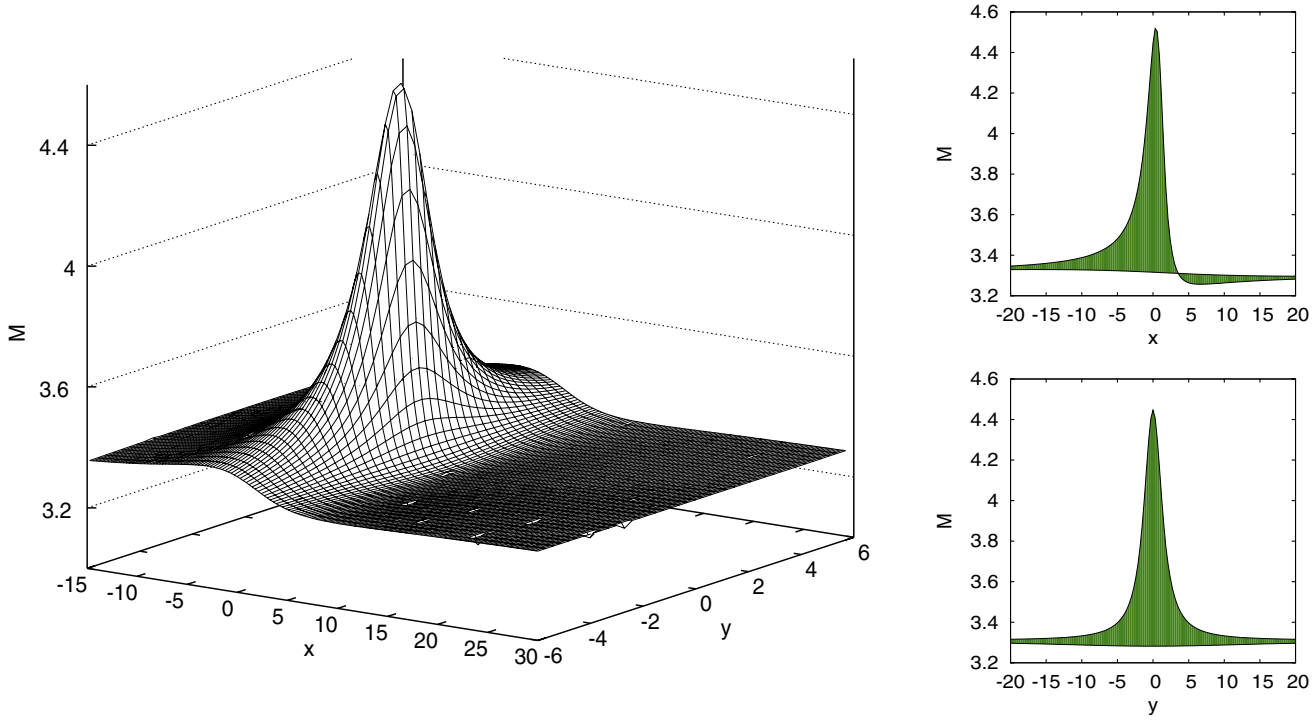

FIG. 2 (color online). Graph of $M(x, y)$ on the AAH in the space $t = 13.0$ (compare Fig. 1). More explanation in the text.

pair (x, y) there will be an M obeying (4.11). The graph shows at which points in the (x, y) plane the AAH has the largest radius (as measured by M), and where it has the smallest radius. The maximum of M is at the intersection of curve AAH+ in Fig. 1 with the line $t = 13.0$; the minimum of M is at the intersection of curve AAH− with the same line. Comparison with Fig. 1 shows that the values of M are indeed all in the expected range. Figure 3 shows the intersection of the AAH with the ordinary AH, which, at $t = 13.0$ is at the mass

$$M \overset{\text{def}}{=} M_{\text{AH}} = 3.82860. \tag{6.6}$$

The coordinates (x, y) are not very intuitive. To better visualize the AAH let us first use the stereographic projection (2.7) to transform (x, y) to the (ϑ, φ) coordinates, and then map the AAH into an abstract Euclidean space with the coordinates (ξ, ψ, ζ). The second transformation has the following form:

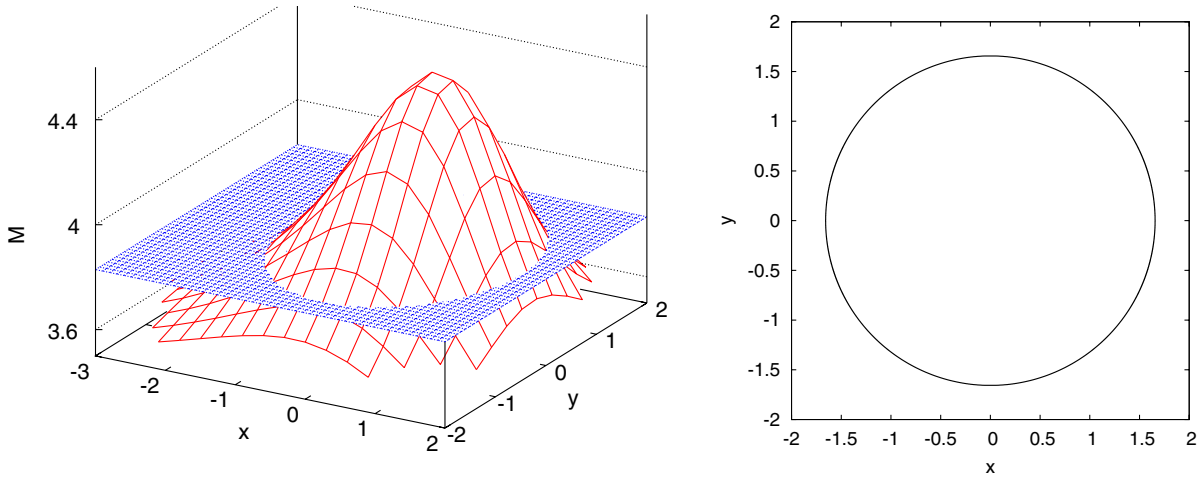

FIG. 3 (color online). *Left*: Intersection of the AAH with the ordinary AH (it lies in the plane $M = 3.82860$) at $t = 13.0$. *Right*: The line of intersection of the AAH with the ordinary AH.

$$\xi = M_{\mathrm{AAH}}(\vartheta,\varphi)\sin\vartheta\cos\varphi, \quad \psi = M_{\mathrm{AAH}}(\vartheta,\varphi)\sin\vartheta\sin\varphi,$$
$$\zeta = M_{\mathrm{AAH}}(\vartheta,\varphi)\cos\vartheta. \tag{6.7}$$

We now use these coordinates to present the evolution of the AAH. As seen from (2.8), when $Q_{,z} = 0$ the extreme values of $\mathcal{E}_{,z}/\mathcal{E}$ with respect to φ are when $\varphi = 0$ and $\varphi = \pi$, which, as follows from (6.7), implies $\psi = 0$. Therefore, Fig. 4 presents the intersection of the AAH with the plane $(\xi, \psi = 0, \zeta)$ at six different time instants.

Note how the lack of spherical symmetry influences the situation. The "origin," where $R = 0$ ($\xi = 0$, $\zeta = 0$), is inside the smallest contour in Fig. 4. The AAH+ first appears off the origin (inside the closed curve in the lower left part of the figure). As seen, at this instant, most rays will miss it. Then it increases in diameter and encroaches on the origin. At the instant corresponding to the lowest point of AAH− in Fig. 1 (see the purple curve in Fig. 4, which presents the AAH just moments before this instant, $t = 11.9772$), the cross section is still connected, but consists of two tangent rings, one inside the other. The point of tangency lies at the minimum of AAH−. From that moment on, the cross section splits into two disjoint contours, the smaller of which becomes progressively smaller with increasing t, and shrinks to a point at the instant corresponding to the minimum of the Big Crunch (inside the smallest ring in Fig. 4).

Figure 4 does not show the cross sections of the ordinary AH because they would obscure the image. The AH first appears shortly after $t = 10.0$ and, at the moment of first appearance, would show in Fig. 4 as a single circle with the center at $(\xi, \zeta) = (0, 0)$ and radius slightly larger than $M = 2$. At later instants, the cross section of the AH splits into two circles, with the centers at the same point. The smaller circle has its radius decreasing as t increases, and shrinks to a point at $t = T_0 + t_{B0} = 12.5$ (the smaller contour of the AAH shrinks to a point at the same instant). The larger circle of the AH keeps increasing, and intersects the larger contour of the AAH (which is not a circle) at two points at every instant.

Three-dimensional surface-plots of the AAH and AH at $t = 11.5$ and $t = 13$ are presented in Figs. 5 and 6. At $t = 11.5$ the Big Crunch singularity has not yet appeared; the AAH is still a connected surface and the AH consists of two disjoint parts—one at $M_{\mathrm{AH}} = 0.783$ and the other at $M_{AH} = 3.199$. Both parts are presented in Fig. 5 (the dotted surfaces), and, as seen, each one has one side inside the AAH and one side outside it (the solid surface). Each part of the AH has the shape of a sphere, while at $t = 11.5$ the AAH has the shape of a ping pong ball depressed on one side.

At $t = 13.0$ the singularity already exists at $R = 0$. Each of AH and AAH consists only of a single surface, which surrounds the singularity. As before, part of the AAH is outside the AH, while the other part is located inside the AH.

Between $t = 11.5$ and $t = 13.0$ there is a period when each of AH and AAH is split into two disjoint parts. We do not provide an illustration for this configuration because it would be unreadable. One can imagine it as the object from Fig. 6 that contains a small-scale copy of itself inside. The small object inside does not intersect with the large one.

Figures 4–6 demonstrate that the AH and AAH do not in fact reveal the whole truth about the future fate of the light

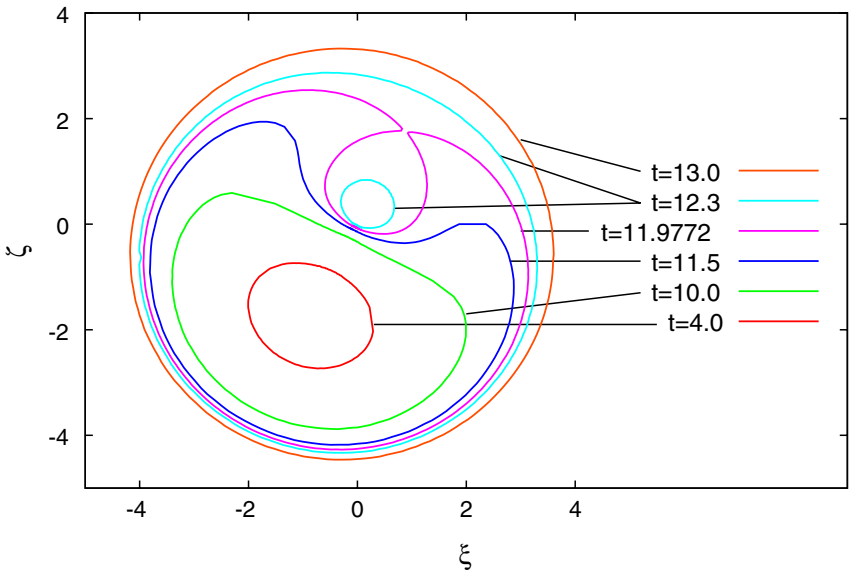

FIG. 4 (color online). The AAH at six different time instants (shown in Fig. 1 as horizontal lines). The curves shown are located on the plane $(\xi, \psi = 0, \zeta)$. This figure can be imagined as a view of Fig. 1 by an observer sitting high on the t-axis and looking down; with one spatial dimension added. The value of M_{AAH} at a point (ξ_0, ζ_0) is the distance between (ξ_0, ζ_0) and the origin $R = 0$, which is inside the smallest contour in the upper right area at $(\xi, \zeta) = (0, 0)$.

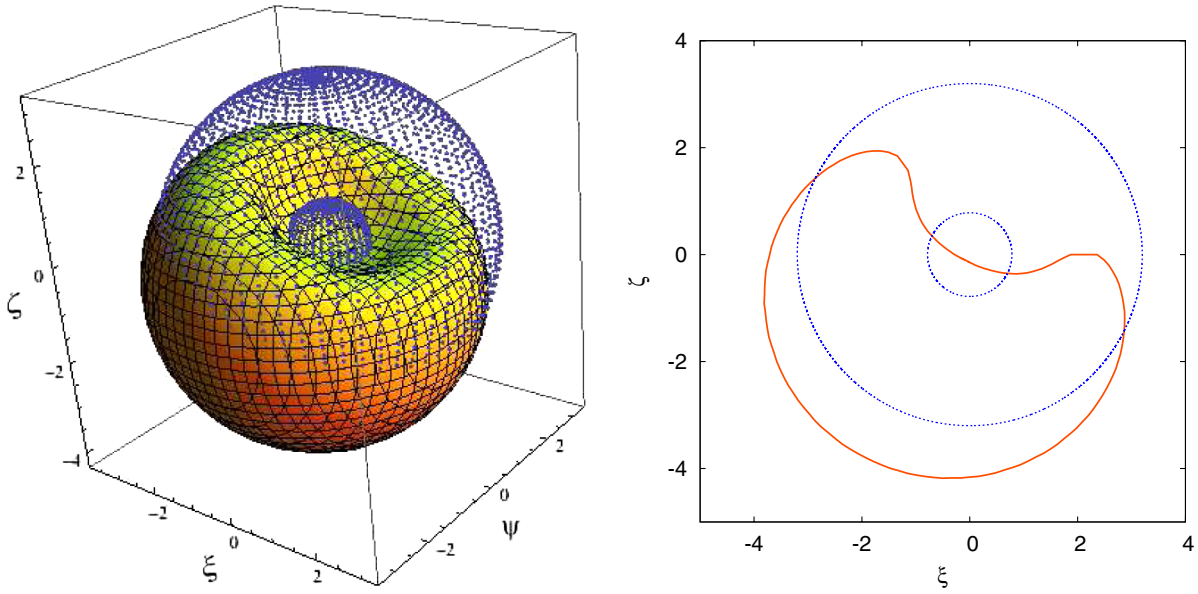

FIG. 5 (color online). *Left*: The M-coordinate on the AAH (solid surface) and AH (dotted surface) represented as a function of ϑ and φ in the space $t = 11.5$. The value of $M(\vartheta, \varphi)$ is the distance of a point on the surface shown from the point $(0, 0, 0)$, in the direction specified by (ϑ, φ). The axes in this picture are in an abstract Euclidean space with coordinates (ξ, ψ, ζ) used only to embed the AAH [see transformation (6.7)]; the (ξ, ψ) do not coincide with the (x, y) of Fig. 2. The (M, ϑ, φ) are spherical polar coordinates in this space. The AH consists of two disjoint spheres—one at $M_{\rm AH} = 0.783$ and the other at $M_{\rm AH} = 3.199$. The origin ($\xi = 0$, $\psi = 0$, $\zeta = 0$) is inside the smaller AAH surface. *Right*: Intersections of the AAH (solid line), and the inner and outer AH (dotted lines) with the plane $(\xi, \psi = 0, \zeta)$ (analogous to Fig. 4).

rays. There exists a region between the $M = 0$ axis and the AAH− in Fig. 1, in which future-directed rays are only formally not yet in the black hole because they are able to proceed outwards. However, they can do so only for a short while. They have no way to avoid intersecting the AAH and the AH in near future, and so they are doomed to hit the Big Crunch.

B. Timelike curves

Equation (4.4) for timelike trajectories is

$$\frac{(R_{,z} - R\mathcal{E}_{,z}/\mathcal{E})^2}{1 + 2E}\left(\frac{\mathrm{d}z}{\mathrm{d}t}\right)^2 = \left[1 - \left(\frac{\mathrm{d}s}{\mathrm{d}t}\right)^2\right] - \frac{R^2}{\mathcal{E}^2}\left[\left(\frac{\mathrm{d}x}{\mathrm{d}t}\right)^2 + \left(\frac{\mathrm{d}y}{\mathrm{d}t}\right)^2\right]. \quad (6.8)$$

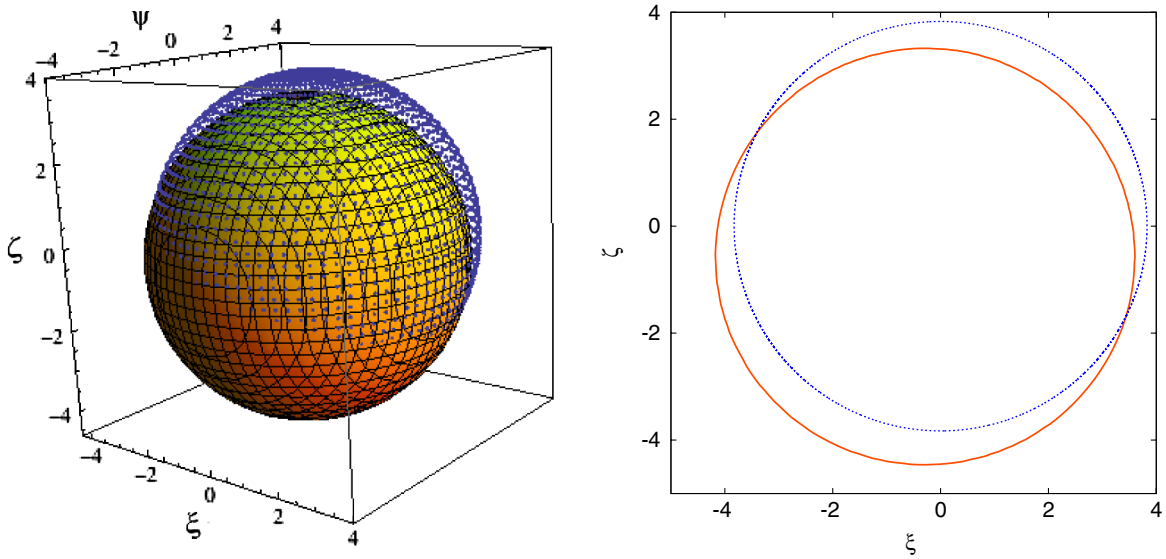

FIG. 6 (color online). The analogue of Fig. 5 at the later instant $t = 13.0$, when the singularity already exists at $R = 0$.

For a trajectory with constant x and y we write

$$\frac{(R_{,z}-R\mathcal{E}_{,z}/\mathcal{E})^2}{1+2E}\left(\frac{\mathrm{d}z}{\mathrm{d}t}\right)^2=\mathcal{V}^2, \tag{6.9}$$

where $\mathcal{V}=\sqrt{1-(\frac{ds}{dt})^2}<1$. Then (4.8) becomes

$$R_{,z}\left(\sqrt{1+2E}-\frac{\sqrt{2M/R+2E}}{\mathcal{V}}\right)+R\frac{\sqrt{2M/R+2E}}{\mathcal{V}}\mathcal{E}_{,z}/\mathcal{E}=0, \tag{6.10}$$

and (4.11) becomes

$$\Psi(\eta)=\left[\left(\frac{M_{,z}}{M}-\frac{E_{,z}}{E}\right)(1-\cos\eta)^{3/2}+\left(\frac{3}{2}\frac{E_{,z}}{E}-\frac{M_{,z}}{M}\right)\frac{\sin\eta(\eta-\sin\eta)}{\sqrt{1-\cos\eta}}-\frac{(-2E)^{3/2}}{M}t_{B,z}\frac{\sin\eta}{\sqrt{1-\cos\eta}}\right]$$
$$\times\left[\sqrt{1+2E}\sqrt{1-\cos\eta}+\frac{\sqrt{-2E}\sin\eta}{\mathcal{V}\sqrt{1-\cos\eta}}\right]-\frac{\sqrt{-2E}}{\mathcal{V}}\sin\eta(1-\cos\eta)\frac{\mathcal{E}_{,z}}{\mathcal{E}}=0. \tag{6.11}$$

Figure 7 is the analogue of Fig. 1 for a particle moving with velocity $\mathcal{V}=0.9$.

VII. WHICH IS THE TRUE HORIZON—AH OR AAH?

To get insight into this question we recall that a quasispherical Szekeres spacetime can be matched to the Schwarzschild spacetime across an $z=b=$ constant hypersurface; this was first proved by Bonnor [6,7]. We recapitulate the basic facts about this matching by the method of Ref. [30].

To verify the matching, the Schwarzschild solution must first be transformed to the Lemaître [26]-Novikov [31] coordinates; see Ref. [18] (Sec. 14.12) for a derivation. In these coordinates, it has the form

$$\mathrm{d}s^2=\mathrm{d}t^2-\frac{R_{,r}^2}{1+2E(r)}\mathrm{d}r^2-R^2(t,r)(\mathrm{d}\vartheta^2+\sin^2\vartheta\mathrm{d}\varphi^2), \tag{7.1}$$

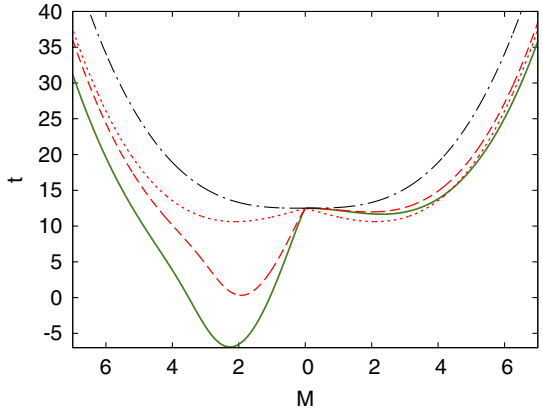

FIG. 7 (color online). Comparison of the AAH of a null ray (dashed lines) with the AAH of a particle moving with velocity $\mathcal{V}=0.9$ (solid lines). The dotted line represents the AH, and the dashed-dotted line represents the big crunch (BC) singularity. As in Fig. 1 the inner curve (closer to BC) is AAH $-$, the outer curve is the AAH $+$.

where $R(t,r)$ is determined by the equation

$$R_{,t}^2=2E(r)+\frac{2m}{R}, \tag{7.2}$$

m being the Schwarzschild mass and $E(r)$ being an arbitrary function. In this form, the Schwarzschild metric is the limit $M_{,r}=0$ of an L-T model, and the limit of constant M, P, Q, S of a quasispherical Szekeres solution.

Further, the coordinates used on a sphere of constant (t,r) in (7.1) must be transformed to those used in (2.1). Suppose the matching is to be done at $r=z=b=$ constant. Then the transformation is

$$\vartheta=2\arctan\left\{\frac{\sqrt{[x-P(b)]^2+[y-Q(b)]^2}}{S(b)}\right\},$$
$$\varphi=\arctan\left[\frac{y-Q(b)}{x-P(b)}\right], \tag{7.3}$$

where $P(b)$, $Q(b)$ and $S(b)$ are the values of the (P,Q,S) from (2.1) at $z=b$. The transformed metric (7.1) is

$$\mathrm{d}s^2=\mathrm{d}t^2-\frac{R_{,r}^2}{1+2E(r)}\mathrm{d}r^2-\frac{R^2(t,r)}{\mathcal{E}_1^2}(\mathrm{d}x^2+\mathrm{d}y^2), \tag{7.4}$$

where

$$\mathcal{E}_1\overset{\text{def}}{=}\frac{S(b)}{2}\left\{\left[\frac{x-P(b)}{S(b)}\right]^2+\left[\frac{y-Q(b)}{S(b)}\right]^2+1\right\}. \tag{7.5}$$

Now it can be easily verified that the matching conditions between (7.4)–(7.5) and (2.1) are fulfilled at any $r=z=b=$ constant, provided that the $E(r)$ of (7.5) and the $E(z)$ of (2.1) have the same value at $r=z=b$, and that both $R(t,b)$ are the same function of t. The latter condition implies

$$M(b)=m, \tag{7.6}$$

where M is the function from (2.2) and m is the Schwarzschild mass from (7.2).

To answer the question asked in the title of this section we need to verify whether the AH is spacelike or otherwise. For the L-T models, this analysis was done in Ref. [28] and repeated in Ref. [18], with the result that

the ingoing part of the AH (around $M = 0$ in Fig. 1)[7] can be any, while the outgoing part can be spacelike and pointwise null, but never timelike. We use the same method here, adapted to the Szekeres geometry, assuming that (2.5) and (2.6) hold.

From (4.3) we find $R_{,t}\,\mathrm{d}t + R_{,z}\,\mathrm{d}z = 2M_{,z}\,\mathrm{d}z$ along the AH, so

$$\left.\frac{\mathrm{d}t}{\mathrm{d}z}\right|_{\mathrm{AH}} = \left.\frac{2M_{,z} - R_{,z}}{R_{,t}}\right|_{\mathrm{AH}}. \tag{7.7}$$

But in the collapse phase $R_{,t} = -\sqrt{2M/R + 2E}$, and along AH $R = 2M$, so

$$\left.\frac{\mathrm{d}t}{\mathrm{d}z}\right|_{\mathrm{AH}} = \left.\frac{R_{,z} - 2M_{,z}}{\sqrt{1 + 2E}}\right|_{R=2M}. \tag{7.8}$$

The equation of the AH is independent of (x, y), so a vector tangent to the AH has only the t- and r- components. We consider an intersection of a (t, r) surface with the light cone at a point of the AH; see Fig. 8. Along a null geodesic that is tangent to this surface at the vertex of the light cone (and so has $\mathrm{d}x/\mathrm{d}t = \mathrm{d}y/\mathrm{d}t = 0$) we have from (5.3)

$$\left.\frac{\mathrm{d}t}{\mathrm{d}z}\right|_{\mathrm{ng/AH}} = \left.\frac{R_{,z} - 2M\mathcal{E}_{,z}/\mathcal{E}}{\sqrt{1 + 2E}}\right|_{\mathrm{ng/AH}}. \tag{7.9}$$

As the lower panel of Fig. 8 shows, the following quantity indicates whether the AH is spacelike or otherwise

$$B \overset{\mathrm{def}}{=} \frac{(\mathrm{d}t/\mathrm{d}z)_{\mathrm{AH}}}{(\mathrm{d}t/\mathrm{d}z)_{\mathrm{ng/AH}}} = \left.\frac{R_{,z} - 2M_{,z}}{R_{,z} - 2M\mathcal{E}_{,z}/\mathcal{E}}\right|_{\mathrm{ng/AH}} \equiv 1 - \left.\frac{2(M_{,z} - M\mathcal{E}_{,z}/\mathcal{E})}{R_{,z} - 2M\mathcal{E}_{,z}/\mathcal{E}}\right|_{\mathrm{ng/AH}}. \tag{7.10}$$

Namely

THE AH IS	WHEN
Outgoing timelike	$B > 1$
Outgoing null	$B = 1$
Spacelike	$-1 < B < 1$
Ingoing null	$B = -1$
Ingoing timelike	$B < -1$

From (2.5) and (2.6) we see that $M_{,z} - M\mathcal{E}_{,z}/\mathcal{E} > 0$ and $R_{,z} - 2M\mathcal{E}_{,z}/\mathcal{E} > 0$ are always fulfilled, so necessarily $B < 1$, i.e., the AH can never be outgoing timelike or null; its outgoing part is necessarily spacelike. The other three possibilities listed in the table are allowed.

As Fig. 1 shows, even if part of the ingoing branch of the AH is timelike, a null curve crossing the AH outwards from the inside will be trapped in the funnel formed by the AAH around $R = 0$. Whether it later crosses the AAH or not, it will be forced to hit the Big Crunch within a finite segment of its affine parameter. Where the AH is spacelike, a null line that crossed it once cannot cross it again without being redirected toward the past. This shows that in its outgoing part the AH acts as a black hole surface, even in that region where the AAH is inside it. The conclusion is that the true horizon is the AH rather than the AAH.

This conclusion is strengthened by the following consideration. If a portion of the Szekeres manifold, of finite spatial diameter, is matched to the Schwarzschild solution, then, from (7.6), the AH matches to the Schwarzschild event horizon. Thus, no signal can escape to infinity if it was within the Szekeres AH while crossing the outer surface at $z = b$. The intersection of the AAH with the outer surface of the Szekeres ball leaves no trace in the Schwarzschild geometry. In particular, this happens in that part of the Szekeres region, where the AAH is earlier than the AH (e.g. in the left half of Fig. 1).

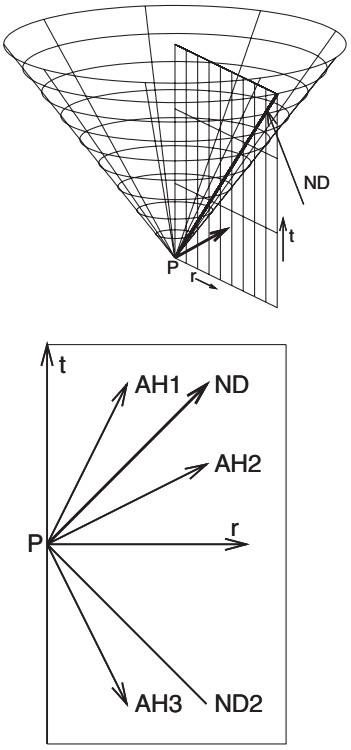

FIG. 8. *Top:* The light cone at a point P on the AH and its intersection with the plane tangent to the (t, r) surface at P. The intersection determines a null direction ND—the thick line. The arrow in the plane marks a hypothetical direction tangent to the AH. *Bottom:* The plane from the upper panel. The figure shows also the past light cone of P (ND2) and three hypothetical directions of the vector tangent to the AH at P. In the position AH1, the AH would be outgoing timelike, in AH2—spacelike (the position marked in the top panel), and with AH3—ingoing timelike. If the direction of AH coincides with ND or ND2, then the AH is null at P. The quantity B defined in (7.10) identifies the various possibilities.

[7]"Ingoing" ("outgoing") mean, respectively, "R decreases (increases) as we proceed along the AH toward increasing t".

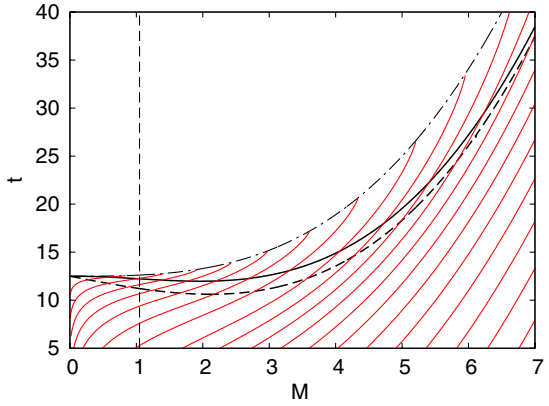

FIG. 9 (color online). A family of the nearly radial null rays defined by (4.5) (thin solid lines). The solid thick line represents the AAH−, the dashed thick line represents the AH, and the dashed-dotted line represents the big crunch (BC) singularity. To the right of the dashed vertical line ($M = 1.048$) the AH is spacelike, to the left it is ingoing timelike.

The above considerations are illustrated in Fig. 9, which shows a family of the nearly radial nongeodesic null lines (NRNL) for the model discussed in Sec. VI A. It is similar to Fig. 1, but for clarity we only show one part of it, where the AH is below the AAH. Calculations[8] showed that, depending on the direction and the value of M, both the AAH and AH can be spacelike or ingoing timelike. Figure 9 shows the behavior in the direction of maximal contribution from $\mathcal{E}_{,z}/\mathcal{E}$. In this direction the AAH− is everywhere spacelike, while the AH is ingoing timelike for $M < 1.048$ (the vertical line in Fig. 9) and spacelike for $M > 1.048$. In other directions parts of the AAH can be timelike. The location of the border between the ingoing timelike and spacelike parts of the AH is direction-dependent, as follows from (7.10). (This is so because the slope of the null cone generator is direction-dependent, as seen from (7.9)). In neither case can the AAH or the AH be outgoing timelike. Thus, even if in some regions radial null rays can propagate toward increasing R, they cannot escape from inside the AH and eventually they cross the AAH.

VIII. SUMMARY

In order to gain a deeper insight into the quasispherical Szekeres geometries we have investigated the spatial relation between the apparent horizon (AH) as defined by Szekeres [2] and the absolute apparent horizon (AAH). The concept of the AAH was first introduced by Hellaby and Krasiński [15], but under the name of AH. In Ref. [15], this spatial relation was investigated at a general level, at which it was not possible to give graphical examples. Such graphical examples are given here in the simple subcase of the Szekeres model defined by (6.1), (6.2), and (6.5). The examples illustrate what was said in Ref. [15], that the AAH "is a kind of oval with half inside $R = 2M$ and half outside." The shape of this "kind of oval" is shown here in Figs. 5 and 6.

An observer who would fall into the region between the surfaces of AAH and AH (top part of Fig. 6 between the solid surface and dotted surface) for a short while would have a chance to send a message some distance outwards (i.e., on a path with increasing R). This is because in a general Szekeres model the hypersurface at which the light rays begin to converge (the AH) does not coincide with the hypersurface at which all rays are forced to proceed toward decreasing areal radius R (the AAH). However, the signal cannot proceed far enough to escape the AH. Moreover, if the Szekeres spacetime is matched to the Schwarzschild spacetime, the AH finds its prolongation in the Schwarzschild event horizon. Consequently, it is the AH that acts as a true horizon.

Whether the concept of AAH can be usefully applied to astrophysical considerations about galactic black holes remains to be seen. For this purpose, the current position of the AH in space, inside the galaxy chosen for observation, would have to be precisely determined, which seems to be a rather remote possibility.

ACKNOWLEDGMENTS

This research was supported by the Polish Ministry of Education and Science Grant No. N N202 104 838 (AK) and the European Union Seventh Framework Programme under Grant No. PIEF-GA-2009-252950 (KB).

APPENDIX A: THE PROOF THAT THE SOLUTION OF (4.11) IS UNIQUE

We prove here that (4.11) is fulfilled by only one value of $\eta \in (\pi, 2\pi)$ for each set of values of (z, x, y).

We begin by recalling the following:

(1) Equation (4.11) that determines $\eta(z, x, y)$ on the AAH is derived from (4.7), and so all quantities in it are calculated along the nearly radial nongeodesic null line (NRNL) that obeys (4.4) with x and y being constant, i.e.,

$$\frac{(R_{,z} - R\mathcal{E}_{,z}/\mathcal{E})^2}{1 + 2E}\left(\frac{\mathrm{d}z}{\mathrm{d}t}\right)^2 = 1. \tag{A1}$$

(2) Note, from (2.3), that

$$\frac{\partial t}{\partial \eta} = \frac{M}{(-2E)^{3/2}}(1 - \cos\eta) > 0 \quad \text{for } \eta \in (0, 2\pi), \tag{A2}$$

at every fixed (z, x, y), so $t(\eta)$ is a monotonic function in this range, i.e. $(\eta_i < \eta_j) \Rightarrow (t(\eta_i) < t(\eta_j))$ for every fixed (z, x, y).

[8] At each point of intersection of the NRNL with the AH and with the AAH we numerically calculated and compared their slopes.

Now suppose that (4.11) has more than one solution for η at a given (z, x, y), and call the solutions $(\eta_1, \ldots, \eta_k)$, with $\eta_1 < \ldots < \eta_k$. Then (A2) implies that there would be k instants $t_1 < \ldots < t_k$, at which the given NRNL would intersect the AAH, all the t_i, $i = 1, \ldots, k$ corresponding to the same (z, x, y) in (4.11). Our supposition thus implies that the inverse function to $t(z, x, y)$ has the property $z(t_1, x, y) = z(t_2, x, y)$. Since this function is continuous (even differentiable, see (A1)), this means that for some $\bar{t} \in (t_1, t_2)$ we have $\mathrm{d}z/\mathrm{d}t|_{t=\bar{t}} = 0$. But from (A1) we have

$$\frac{\mathrm{d}z}{\mathrm{d}t} = \pm \frac{\sqrt{1 + 2E}}{R_{,z} - R\mathcal{E}_{,z}/\mathcal{E}}. \tag{A3}$$

This can be zero only where $E = -1/2$. This set is a neck [18]—an analogue of the Kruskal-Szekeres wormhole in the Schwarzschild solution. i.e., a special location in spacetime that may or may not exist, depending on whether E attains the value $-1/2$ anywhere.

Thus, for every NRNL obeying (A1) that does not traverse a neck, $\mathrm{d}z/\mathrm{d}t \neq 0$ everywhere along it. This means that $z(t_1, x, y) = z(t_2, x, y)$ cannot happen, i.e., that (4.11) has only one solution for η at each given (z, x, y). □

APPENDIX B: THE LIMIT OF AAH AT THE CENTER $M = 0$

For the numerical calculation we need to know the value of the function $t(M)_{\mathrm{AAH}}$ in (4.12) at $M = 0$. This has to be calculated exactly because numerical programs are unreliable in calculating limits. From (6.1) and (6.3) we have

$$\lim_{M\to 0} t_B(M) = t_{B0}, \qquad \lim_{M\to 0} \frac{M}{(-2E)^{3/2}} = \frac{T_0}{2\pi}, \tag{B1}$$

so

$$\lim_{M\to 0} t(M)_{\mathrm{AAH}} = t_{B0} + \frac{T_0}{2\pi} \lim_{M\to 0} (\eta - \sin\eta). \tag{B2}$$

In order to calculate $\lim_{M\to 0}\eta$ we use (4.11). Equation (4.15) shows that $\sin\eta/\sqrt{1-\cos\eta}$ is finite in the full range $\eta \in [0, 2\pi]$. We take M as the z-coordinate and observe from (2.1) that with (P, Q, S) given by (6.5), $\mathcal{E}_{,M}/\mathcal{E}$ will be finite at $M = 0$. Then, substituting (6.1) and (6.3) in (4.11) we get

$$\lim_{M\to 0} \Psi(\eta) = \lim_{M\to 0} \frac{(1-\cos\eta)^2}{3M} = 0 \tag{B3}$$

(because $\Psi(\eta) = 0$ all along the AAH). This is possible only when $\lim_{M\to 0}\cos\eta = 1$, which, in the collapse phase, means

$$\lim_{M\to 0} \eta = 2\pi. \tag{B4}$$

Using this in (B2) we obtain

$$\lim_{M\to 0} t(M)_{\mathrm{AAH}} = t_{B0} + T_0 = \lim_{M\to 0} t_C(M), \tag{B.5}$$

i.e., the AAH at $M = 0$ coincides with the Big Crunch.

[1] P. Szekeres, Commun. Math. Phys. **41**, 55 (1975).
[2] P. Szekeres, Phys. Rev. D **12**, 2941 (1975).
[3] W. B. Bonnor and N. Tomimura, Mon. Not. R. Astron. Soc. **175**, 85 (1976).
[4] S. W. Goode and J. Wainwright, Mon. Not. R. Astron. Soc. **198**, 83 (1982).
[5] S. W. Goode and J. Wainwright, Phys. Rev. D **26**, 3315 (1982).
[6] W. B. Bonnor, Nature (London) **263**, 301 (1976).
[7] W. B. Bonnor, Commun. Math. Phys. **51**, 191 (1976).
[8] W. B. Bonnor, A. H. Sulaiman, and N. Tomimura, Gen. Relativ. Gravit. **8**, 549 (1977).
[9] M. M. de Souza, Rev. Bras. Fiz. **15**, 379 (1985).
[10] W. B. Bonnor, Classical Quantum Gravity **3**, 495 (1986).
[11] W. B. Bonnor and D. J. R. Pugh, South African Journal of Physics **10**, 169 (1987).
[12] P. Szekeres, in *Gravitational Radiation, Collapsed Objects and Exact Solutions.*, edited by C. Edwards., Lecture Notes Vol. 124 (Springer, New York 1980), p. 477.
[13] K. Bolejko, Phys. Rev. D **73**, 123508 (2006).
[14] K. Bolejko, Phys. Rev. D **75**, 043508 (2007).
[15] C. Hellaby and A. Krasinski, Phys. Rev. D **66**, 084011 (2002).
[16] K. Bolejko, A. Krasiński, C. Hellaby, and M.-N. Célérier, *Structures in the Universe by Exact Methods-Formation, Evolution, Interactions.* (Cambridge University Press, Cambridge, England, 2010.
[17] A. Krasiński and K. Bolejko, Phys. Rev. D **83**, 083503 (2011).
[18] J. Plebański and A. Krasiński, *An Introduction to General Relativity and Cosmology* (Cambridge University Press Cambridge, England, 2006).
[19] A. Krasiński, *Inhomogeneous Cosmological Models* (Cambridge University Press, Cambridge, England, 1997).
[20] K. Bolejko and R. A. Sussman, Phys. Lett. B **697**, 265 (2011).
[21] R. A. Sussman and K. Bolejko, Classical Quantum Gravity **29**, 065018 (2012).
[22] S. A. Hayward, Phys. Rev. D **49**, 6467 (1994).
[23] J. M. M. Senovilla, Int. J. Mod. Phys. D **20**, 2139 (2011).

[24] S. W. Hawking and G. F. R. Ellis, *The Large-Scale Structure of Spaceetime.* (Cambridge University Press, Cambridge 1973).
[25] B. C. Nolan and U. Debnath, Phys. Rev. D **76**, 104046 (2007).
[26] G. Lemaître, Ann. Soc. Sci. Bruxelles A **53**, 51 (1933); English translation, with historical comments: Gen. Relativ. Gravit. **29**, 637 (1997).
[27] R. C. Tolman, Proc. Natl. Acad. Sci. U.S.A. **20**, 169 (1934); reprinted, with historical comments: Gen. Relativ. Gravit. **29**, 931 (1997).
[28] A. Krasiński and C. Hellaby, Phys. Rev. D **69**, 043502 (2004).
[29] C. Hellaby, J. Math. Phys. (N.Y.) **37**, 2892 (1996).
[30] C. Hellaby and A. Krasiński, Phys. Rev. D **77**, 023529 (2008).
[31] I. D. Novikov, Soobshcheniya GAISh [Communications of the State Shternberg Astronomical Institute] **132**, 3 (1964); English translation, with historical comments: Gen. Relativ. Gravit. **33**, 2255 (2001).